Impropriety-Based Multiantenna Spectrum Sensing with I/Q Imbalanced Radios

Amir Zaimbashi, *Member, IEEE* and Mikko Valkama, *Senior Member, IEEE*

***Abstract*—Direct conversion radios are widely recognized as the most appealing approach for reducing the hardware cost as well as power consumption in upcoming communication systems. However, such radios are known to entail gain and phase uncertainties along the analog inphase/quadrature (I/Q) paths. In this article, we address the effects of the transmitter (TX) and receiver (RX) I/Q errors or mismatches on the improperness of the transmitted and received signals, respectively. We analytically show how the properness of a transmitted signal and the receiver thermal noise can be destroyed, respectively, under the transmitter and receiver I/Q errors, given that the corresponding ideal signals are proper under perfect I/Q balance. Then, we address the spectrum sensing problem in cognitive radio systems, through modelling it as a composite binary hypothesis testing task, and apply the likelihood ratio test (LRT) approach to solve it. To this end, we propose three impropriety-based multiantenna spectrum sensing algorithms under the transmitter and receiver I/Q uncertainties. The principle of invariance is exploited to examine the potential constant false alarm rate (CFAR) behavior of the proposed detectors. We analytically prove that all the proposed sensing methods posses CFAR behavior against the noise variance uncertainty, while only two of them have CFAR property against the receiver I/Q mismatch values. The achievable sensing performance of the proposed methods is then analyzed through extensive numerical experiments, and the devised alternative detectors are mutually compared. Finally, analytical solutions are derived to quantify the improvement/degradation in the effective received signal SNR under I/Q imbalanced radios.**

***Index Terms*—Spectrum sensing, cognitive radio, improper/ proper random signals, I/Q imbalance, likelihood ratio test, CFAR property, invariance, multiantenna receivers.**

I. Introduction

It is commonly understood and agreed that the radio frequency (RF) spectrum is used relatively inefficiently [1]- [2]. This is mainly stemming from the heavily varying demands and requirements of the so called primary users (PUs), which typically use only subsets of the licensed spectrum. Therefore, cognitive radio (CR) is widely considered as a promising and effective approach to enhance the spectrum utilization efficiency and thus to potentially relax the problem of spectrum scarcity [1]- [4]. The basic idea of CR is to allow secondary users (SUs) to dynamically deploy the temporally or geographically unused spectral resources of the primary users (PUs). To do this, SUs need to conduct reliable spectrum sensing to determine whether or not a certain spectral resource is being utilized by PUs. If SUs detect unused spectral resources, they can opportunistically pursue cognitive channel access and radio transmission. In these cases, there is no interference between SUs and PUs, realizing an interweave spectrum sharing mode [5], [6]. If all the spectral resources are utilized by the PUs, SUs can either collect more information in terms of, e.g., channel responses and power levels, to realize overlay spectrum sharing or alternatively, conduct cognitive transmissions and realize underlay spectrum sharing strategy [5], [6]. All of these infer that the spectrum sensing is a keying problem and task in CR systems and networks. For clarity, we note that opportunistic sensing based channel access schemes are best suited for delay-tolerant traffic scenarios.

A. Zaimbashi is with Shahid Bahonar University of Kerman, Kerman, Iran (e-mail: a.zaimbashi@uk.ac.ir).

M. Valkama is with Tampere University, Tampere, Finland (e-mail: mikko.valkama@tuni.fi).

A. Related Work

In the existing literature, tremendous amount of work and efforts have been invested in the development of accurate and reliable spectrum sensing algorithms, see, e.g., [7]- [14]. Most of the existing works do not, however, consider the practical impairments associated with the analog baseband and radio frequency (RF) circuits. Good example of such impairments are the so-called in-phase/quadrature (I/Q) errors observed in the direct-conversion radio transmitters (DCT) and receivers (DCR) [15], [16], stemming from the relative gain and phase uncertainties along the analog I and Q paths [17]- [21]. Such mismatches arise due to the deficiencies of the analog baseband and RF front-end modules of a transceiver, such as filtering, mixing and amplification stages, as well as data converter interfaces, and cannot be avoided in practical circuit solutions and implementations.

Existing literature has showed that RX I/Q imbalance can induce impropriety in both modulated signals and noise [22]- [24]. In this article, we obtain closed-form analytical expressions for the level or degree of impropriety of both the transmitted signal as well as the received signal components under I/Q imbalanced radios. The derived expressions then allow us to assess and quantify the effects of the TX and RX I/Q imbalances on the impropriety degree of the different received signal components.

When it comes to spectrum sensing in CR systems, the performance degradation stemming from the TX and RX I/Q imbalances has been investigated in [25]- [31]. Most of the existing works have treated improper signals due to RX I/Q imbalance as proper ones to deduce spectrum sensing algorithms [25]- [31]. In our previous work [32], we addressed the improper features of the modulated waveform and observable noise, but utilized a digital calibration stage to mitigate the receiver I/Q uncertainties. Such approach essentially re-circularizes the processed received signal, and thus ordinary detector can be applied. While the work in [32] serves as the background and starting point, this article addresses a more

challenging and generic case of co-existing joint transmitter and receiver I/Q uncertainties and also assumes that we are dealing with a non-calibrated receiver. Hence, also the spectrum sensing algorithms need to be redesigned.

Our aim in this article is to exploit the improper features of the observed signal at received side, arising from the coexisting transmitter and receiver uncertainties, to improve the spectrum sensing capabilities in CR networks. To facilitate that, and to enhance the spectrum sensing reliability, we assume that multiple antennas are deployed at SUs. To this end, we specifically address a Single-Input Multiple-Output (SIMO) opportunistic radio access scenario with specific emphasis on the spectrum sensing task within a given frequency channel. Towards that end, we pursue detectors that posses the so called constant false alarm rate (CFAR) characteristics, while also assume different noise variances in the individual receiver chains of the multiantenna sensing RX, for generality. For clarity, we state that our work focuses on non-cooperative spectrum sensing, while various cooperative sensing and cooperative spectrum sharing methods also exist in the literature, see, e.g., [14] and the references therein.

B. Main Contributions

This article considers the non-cooperative spectrum sensing task in a single-channel SIMO CR configuration when both the TX and RX radios suffer from I/Q imbalances. Differently from previous works, we consider the received signal components (both signal and noise) as improper signals. The main contributions of this article can be summarized as follows:

- The received signal model under the coexisting joint transmitter and receiver I/Q uncertainties is developed, serving as the basis for spectrum sensing. We observe that I/Q imbalances can, in general, induce improper features in both the modulated waveform and observable noise. We then analytically quantify the impropriety degree of the received signal as a function of the transmitter and receiver I/Q mismatch values. Under realistic levels of I/Q errors, we show that the degree of impropriety is low when we use a proper signal modulation for transmission, while it may be high for improper or maximally improper signals.
- The spectrum sensing task under I/Q imbalances is formulated as a composite binary hypothesis testing problem, and solved through a likelihood ratio test (LRT) approach. Specifically, we devise three spectrum sensing algorithms based on different assumptions about the impropriety or propriety of the desired and noise signals. However, a substantial body of this work focuses on the design of spectrum sensing algorithms to exploit the potential improper features of the observed signal.
- The principle of invariance is exploited to examine the potential CFAR behavior of the proposed detectors against noise variance uncertainty (NVU) as well as against receiver I/Q mismatch values. The obtained analytical results show that all the proposed sensing methods posses CFAR behavior against the noise variance uncertainty, while two of them have CFAR property also with respect to the receiver I/Q error characteristics.
- Building on the general model for transceiver I/Q uncertainties described in [33], we obtain a closed-form analytical expression for the received signal-to-noise ratio (SNR) under I/Q imbalanced radios. The effective received SNR is shown to be a product of the input SNR and the TX and RX SNR factors, revealing the impacts of the transmitter and receiver I/Q amplitude and phase uncertainties on the detection performance and its potential improvement/degradation.
- The performance of the proposed detectors is analyzed and mutually compared. The results show that it is not necessary to take into account the impropriety nature of the received signals when the degree of impropriety is small. However, if the underlying signal modulations are improper, large performance gains are available if the impropriety of desired signal and noise are taken into account in designing the spectrum sensing algorithms.
- The performance of the proposed method is also compared, in terms of the receiver operating characteristics (ROC) curves, against known state-of-the-art reference methods [9], [10], [34] and [35], that do not consider the potential improper nature of the signals. The results clearly demonstrate the benefits of the proposed methods.

C. Paper Organization and Notations

The rest of this article is organized as follows. In Section II, selected preliminaries about improper/proper random variables are first reviewed. Then, the essential received signal model in the considered SIMO CR scenario under coexisting transmitter and receiver I/Q errors is developed and described. In Section III, the fundamental spectrum sensing task is formulated as a composite binary hypothesis testing problem, building on the derived received signal models. In addition, it is discussed and addressed how the I/Q mismatches impact the properness of the transmitted and received signals and observable noise. Then, three new spectrum sensing algorithms are proposed and derived, addressing different cases and assumptions about the proper/improper nature of the received signal and noise terms. The CFAR properties of the proposed detectors are analytically addressed in Section IV. Finally, extensive numerical examples are provided and analyzed in Section V, while the concluding remarks are then provided in Section VI.

In the following, $(.)^T$, $(.)^*$, and $(.)^H$ denote the transpose, complex conjugate and the Hermitian (conjugate transpose), respectively. All vectors and matrices are denoted by bold lower case and bold upper case letters, respectively. For a square matrix $\mathbf{A}$, $|\mathbf{A}|$ denotes the determinant, while $[\mathbf{A}]_{m,n}$ refers to its mnth element. Similarly, for vector $\mathbf{a}$, a_m represents its mth element. diag($\mathbf{a}$) refers to a square matrix with the elements of $\mathbf{a}$ along its main diagonal and zeros everywhere else, while Diag($\mathbf{A}$) denotes a square matrix of the diagonal elements of $\mathbf{A}$ along its main diagonal and zeros everywhere else. $\mathbf{I}_k$ is the identity matrix of size k. $\mathbf{0}_{m\times n}$ represents the all-zeros matrix of size $m \times n$, while $\mathbf{1}_{m\times n}$ represents the all-ones matrix of size $m \times n$. The operators $E\{.\}$, $\Re\{.\}$, $*$, $\otimes$ and $\odot$ denote the expectation, the real part, the convolution, the Kronecker product and the Hadamard product, respectively. Finally, the imaginary unit is defined as $j = \sqrt{-1}$.

II. Problem Formulation

A. Basics and Preliminaries

Consider a complex-valued random vector $\mathbf{x} \in \mathcal{C}^M$ with zero-mean whose ordinary covariance matrix is defined as $\mathbf{R} = E\{\mathbf{x}\mathbf{x}^H\}$ while the complementary covariance matrix (sometimes also referred to as the relation function or pseudo-covariance) is defined as $\tilde{\mathbf{R}} = E\{\mathbf{x}\mathbf{x}^T\}$ [36].

Definition 1. *The complex random vector* $\mathbf{x}$ *is proper if* $\tilde{\mathbf{R}} = \mathbf{0}$ *and improper if* $\tilde{\mathbf{R}} \neq \mathbf{0}$ *[36].*

Definition 2. *The general probability density function (pdf) of a zero-mean improper Gaussian random vector* $\mathbf{x}$ *is given by [36]:*

$$f(\mathbf{x}) = \frac{1}{\pi^M |\underline{\mathbf{R}}|^{1/2}} \exp\{-\frac{1}{2}\underline{\mathbf{x}}^H \underline{\mathbf{R}}^{-1}\underline{\mathbf{x}}\} \tag{1}$$

where $\underline{\mathbf{x}} = [\mathbf{x}^T, \mathbf{x}^H]^T \in \mathcal{C}^{2M}$ *denotes the augmented observation vector while* $\underline{\mathbf{R}}$ *represents the augmented covariance matrix given by*

$$\underline{\mathbf{R}} = \begin{bmatrix} \mathbf{R} & \tilde{\mathbf{R}} \\ \tilde{\mathbf{R}}^* & \mathbf{R}^* \end{bmatrix} \in \mathcal{C}^{2M\times 2M} \tag{2}$$

For proper/circular complex Gaussian random vector $\mathbf{x}$*, (1) reduces to*

$$f(\mathbf{x}) = \frac{1}{\pi^M |\mathbf{R}|} \exp\{-\mathbf{x}^H \mathbf{R}^{-1}\mathbf{x}\} \tag{3}$$

This is followed form the fact that a complex random vector $\mathbf{x}$ *is defined proper iff* $\mathbf{x}$ *and its conjugate* $\mathbf{x}^*$ *are uncorrelated implying* $\tilde{\mathbf{R}} = \mathbf{0}$*.*

B. Signal Model

The basic considered system model with a single-antenna PU transmitter and a multi-antenna SU sensing receiver, with M antennas and receiver chains, is shown in Fig. 1(a). All associated transmit and receive chains are assumed to be subject to I/Q imbalances, as indicated in the figure. Now, assuming that the PU transmitter is active, the sampled baseband equivalent received signal corresponding to the m-th antenna branch at the SU side can be written as

$$r_m[n] = h_m s[n] + w_m[n], \tag{4}$$

for $n = 1, ..., N$, with N denoting the number of available samples corresponding to the sensing window. In (4), h_m denotes the flat fading [7], [28] complex baseband equivalent channel from the PU transmit antenna to the m-th receiving antenna of the SU, while $s[n]$ denotes the transmitted complex baseband signal. Additionally, quasi-static assumption is deployed [7] meaning that the channel variables h_m stay constant over the sensing window while can vary from sensing window to another. Also, the distribution of the noise $w_m[n]$ is assumed to be circularly symmetric complex Gaussian (CSCG) with zero mean.

Based on the frequency-independent model of [33], the transmitted signal $s[n]$ impaired by TX I/Q imbalance can be represented as [32], [33]

$$s[n] = k_1^t p[n] + k_2^t p^*[n], \tag{5}$$

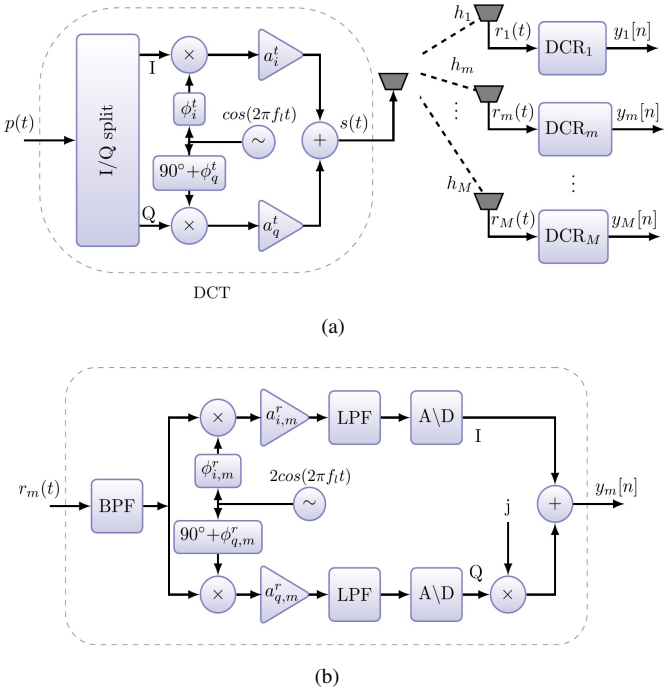

Fig. 1. In (a), the considered SIMO cognitive radio system is shown, while (b) illustrates a model of a direct-conversion receiver under I/Q imbalance.

where $p[n]$ denotes the ideal complex baseband equivalent transmit signal. From (5), one can observe that $p[n]$ is subject to distortion by the so called image signal $p^*[n]$, arising due to the TX I/Q imbalance. Let ϕ_i^t, ϕ_q^t and a_i^t, a_q^t denote the phase and gain deviations of the I and Q channels relative to the nominal ones. As a result, the TX I/Q imbalance coefficients k_1^t and k_2^t read

$$k_1^t = 0.5 a_i^t e^{j\phi_i^t}(1 + \eta_t e^{j\Delta\phi_t}), \tag{6}$$

$$k_2^t = 0.5 a_i^t e^{j\phi_i^t}(1 - \eta_t e^{j\Delta\phi_t}), \tag{7}$$

where η_t and $\Delta\phi_t$ are the gain and phase mismatches between the I and Q paths, i.e., $\eta_t = \frac{a_q^t}{a_i^t}$ and $\Delta\phi_t = \phi_q^t - \phi_i^t$. In a similar manner, the RX I/Q imbalance impacts the basic received signal model in (4) through the following transformation [33]

$$y_m[n] = k_{1,m}^r r_m[n] + k_{2,m}^r r_m^*[n], \tag{8}$$

where $r_m[n]$ refers to the received complex baseband equivalent signal under perfect RX I/Q balance. In (8), $k_{1,m}^r$ and $k_{2,m}^r$ are the I/Q imbalance coefficients of the m-th receiver defined as

$$k_{1,m}^r = 0.5 a_{i,m}^r e^{-j\phi_{i,m}^r}(1 + \eta_m^r e^{-j\Delta\phi_m^r}), \tag{9}$$

$$k_{2,m}^r = 0.5 a_{i,m}^r e^{j\phi_{i,m}^r}(1 - \eta_m^r e^{+j\Delta\phi_m^r}), \tag{10}$$

where $\phi_{i,m}^r$, $\phi_{q,m}^r$ and $a_{i,m}^r$, $a_{q,m}^r$ denote the phase and gain deviations of the I and Q channels, compared to the nominal ones, respectively. Thus, η_m^r and $\Delta\phi_m^r$ represent the RX gain and phase mismatches between the I and Q paths, i.e., $\eta_m^r = \frac{a_{q,m}^r}{a_{i,m}^r}$ and $\Delta\phi_m^r = \phi_{q,m}^r - \phi_{i,m}^r$. From (8), one can deduce that the received signal is also subject to its own image which in this case contains both the PU signal, after having traveled through the channel, as well as noise.

Let now $\mathbf{y}[n] = [y_1[n], \ldots, y_M[n]]^T$ represent the array observation at SU RX. Then, based on (8) and (4) we can write

$$\mathbf{y}[n] = \mathbf{H}\underline{\mathbf{s}}[n] + \mathbf{v}[n], \tag{11}$$

in which $\mathbf{H} = [\mathbf{k}_1 \odot \mathbf{h}, \mathbf{k}_2 \odot \mathbf{h}^*]$, $\mathbf{h} = [h_1, \ldots, h_M]^T$ and $\mathbf{k}_i = [k^r_{i,1}, \ldots, k^r_{i,M}]^T$ for $i = 1, 2$. In above, the observable noise vector $\mathbf{v}[n]$ reads $\mathbf{v}[n] = \mathbf{k}_1\mathbf{w}[n] + \mathbf{k}_2\mathbf{w}^*[n]$, where $\mathbf{w}[n]$ denotes the array thermal noise whose elements are statistically independent and identically distributed (i.i.d.) circularly symmetric complex Gaussians, specifically $\mathbf{w}[n] \sim \mathcal{CN}(\mathbf{0}, \mathbf{\Sigma})$. The noise variance σ_i^2 can in practice differ from σ_j^2 for $i \neq j$ due to the receiver calibration uncertainties. Additionally, the exact noise variances are generally unknown. In (11), the augmented transmit signal vector $\underline{\mathbf{s}}[n] = [s[n], s^*[n]]^T$ reads

$$\underline{\mathbf{s}}[n] = \begin{bmatrix} k_1^t p[n] + k_2^t p^*[n] \\ {k_1^t}^* p^*[n] + {k_2^t}^* p[n] \end{bmatrix} \in \mathcal{C}^{2\times 1} \tag{12}$$

In what follows, we use similar underline-based notations for augmented vector and matrix variables.

III. Spectrum Sensing and Impropriety

In the following, we denote the augmented array observation as $\underline{\mathbf{y}}[n] = [\mathbf{y}[n]^T, \mathbf{y}[n]^H]^T$. The corresponding augmented received signal matrix is, in turn, defined as $\underline{\mathbf{Y}} = [\mathbf{Y}^T, \mathbf{Y}^H]^T = [\underline{\mathbf{y}}[0], .., \underline{\mathbf{y}}[N-1]]$, where $\mathbf{Y} = [\mathbf{y}[1], \ldots, \mathbf{y}[N]]$ denotes an $M \times N$ matrix of the received signal samples. Now, the spectrum sensing task can be interpreted and written as a composite binary detection problem, with the corresponding hypotheses reading

$$\begin{cases} H_0 : \underline{\mathbf{y}}[n] = \underline{\mathbf{v}}[n], \\ H_1 : \underline{\mathbf{y}}[n] = \underline{\mathbf{H}}\underline{\mathbf{s}}[n] + \underline{\mathbf{v}}[n]. \end{cases} \tag{13}$$

In above hypothesis H_1, the extended array channel $\underline{\mathbf{H}}$ is defined as

$$\underline{\mathbf{H}} = \begin{bmatrix} \mathbf{k}_1 \odot \mathbf{h} & \mathbf{k}_2 \odot \mathbf{h}^* \\ \mathbf{k}_2^* \odot \mathbf{h} & \mathbf{k}_1^* \odot \mathbf{h}^* \end{bmatrix} \tag{14}$$

In (13), the null hypothesis H_0 stands for the absence of the PU signal while the alternate hypothesis H_1 corresponds to the PU signal being present.

In the following, we first show that the noise vector $\underline{\mathbf{v}}[n]$ and the desired signal vector $\underline{\mathbf{s}}[n]$ are both improper. Therefore, both the ordinary and the complementary covariance matrices are needed to fully characterize the second-order statistics of the received signal components. Then, we solve the considered spectrum sensing problem through the likelihood ratio test (LRT) approach. In this work, in the detector developments, we consider the amplitude and phase mismatches of the involved indiviudal radio transmitters and receivers as unknown but deterministic constants.

A. Impropriety of Observed Noise and Signal Terms

Let $\underline{\mathbf{v}}[n] = [\mathbf{v}[n]^T, \mathbf{v}[n]^H]^T$ denote the augmented vector of the nth column of the noise matrix $\mathbf{V}$, given by

$$\underline{\mathbf{v}}[n] = \begin{bmatrix} \mathbf{k}_1\mathbf{w}[n] + \mathbf{k}_2\mathbf{w}^*[n] \\ \mathbf{k}_1^*\mathbf{w}^*[n] + \mathbf{k}_2^*\mathbf{w}[n] \end{bmatrix} \in \mathcal{C}^{2M\times 1} \tag{15}$$

Based on (1), we have

$$f(\mathbf{v}[n]) = \frac{1}{\pi^M |\underline{\mathbf{R}}_v|^{1/2}} \exp\{-\frac{1}{2}\underline{\mathbf{v}}[n]^H \underline{\mathbf{R}}_v^{-1} \underline{\mathbf{v}}[n]\} \tag{16}$$

where $\underline{\mathbf{R}}_v = E\{\underline{\mathbf{v}}[n]\underline{\mathbf{v}}[n]^H\}$ corresponds to the augmented noise covariance matrix. Based on (15), combined with straight-forward derivations, the augmented covariance can expressed as

$$\underline{\mathbf{R}}_v = \begin{bmatrix} (\mathbf{k}_1\mathbf{k}_1^H + \mathbf{k}_2\mathbf{k}_2^H) \odot \mathbf{\Sigma} & 2\mathbf{k}_1\mathbf{k}_2^T \odot \mathbf{\Sigma} \\ 2\mathbf{k}_1^*\mathbf{k}_2^H \odot \mathbf{\Sigma} & (\mathbf{k}_1^*\mathbf{k}_1^T + \mathbf{k}_2^*\mathbf{k}_2^T) \odot \mathbf{\Sigma} \end{bmatrix} \tag{17}$$

where we have utilized the fact that the physical array noise is circular or proper. Since $\mathbf{\Sigma} = \text{diag}(\sigma_1^2, ..., \sigma_M^2)$, $\underline{\mathbf{R}}_v$ can be rewritten as

$$\underline{\mathbf{R}}_v = \begin{bmatrix} \text{diag}(\mathbf{z}) & \text{diag}(\mathbf{u}) \\ \text{diag}(\mathbf{u}^*) & \text{diag}(\mathbf{z}) \end{bmatrix} \tag{18}$$

where $\mathbf{z} = [z_1, ..., z_M]^T$ and $\mathbf{u} = [u_1, ..., u_M]^T$, with

$$z_m = 0.5a^r_{i,m}(1 + {\eta^r_m}^2)\sigma_m^2 \tag{19}$$

$$u_m = 0.5a^r_{i,m}(1 - 2j\eta^r_m \sin(\Delta\phi^r_m) - {\eta^r_m}^2)\sigma_m^2 \tag{20}$$

for $m = 1, ..., M$.

From (20), it can be observed that the augmented covariance matrix of observed noise is not diagonal when the RX side radios are subject to I/Q imbalances. In general, to measure and quantify the degree of impropriety of a complex noise vector $\mathbf{v}[n]$, several functions have been proposed to be plausible [37], such as

$$\xi_v = 1 - \frac{|\underline{\mathbf{R}}_v|}{|\underline{\mathbf{R}}'_v|} \tag{21}$$

where

$$\underline{\mathbf{R}}'_v = \begin{bmatrix} \text{diag}(\mathbf{z}) & \mathbf{0}_{M,M} \\ \mathbf{0}_{M,M} & \text{diag}(\mathbf{z}) \end{bmatrix} \tag{22}$$

If $\xi_v = 0$, the observable array noise $\mathbf{v}[n]$ is said to be proper/circular, while for $\xi_v = 1$, we have maximally improper/noncircular noise. Using now the fact that

$$\left| \begin{bmatrix} \mathbf{A} & \mathbf{B} \\ \mathbf{C} & \mathbf{D} \end{bmatrix} \right| = |\mathbf{A}| \left|\mathbf{D} - \mathbf{C}\mathbf{A}^{-1}\mathbf{B}\right|, \tag{23}$$

assuming that $\mathbf{A}^{-1}$ exist, we can re-express (21) as

$$\xi_v = 1 - |\mathbf{I}_M - \text{diag}(\mathbf{z})^{-1}\text{diag}(\mathbf{u}^*)\text{diag}(\mathbf{z})^{-1}\text{diag}(\mathbf{u})| \tag{24}$$

Combining our results so far, we can obtain

$$\xi_v = 1 - \prod_{m=1}^{M} d_m^2 \tag{25}$$

where

$$d_m = \frac{2\eta^r_m \cos(\Delta\phi^r_m)}{1 + {\eta^r_m}^2} \tag{26}$$

It is thus seen that ξ_v depends on the number of receive antennas as well as the gain and phase mismatches across the different RX chains. As expected, an array sensing device combined with zero I/Q errors in all the associated receivers corresponds to $\eta^r_m = 1$, $\Delta\phi^r_m = 0$, for all m, and thus

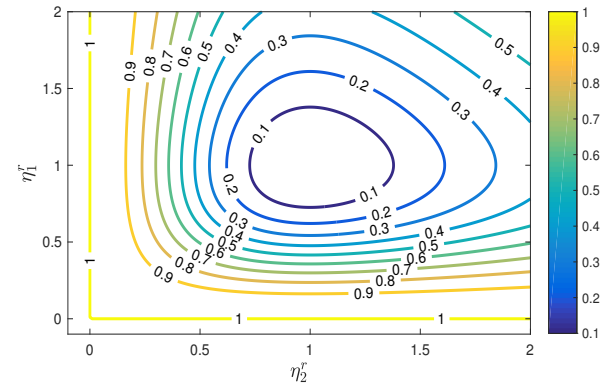

(a) $(\Delta\phi_1^r, \Delta\phi_2^r) = (2, -3)$ degrees

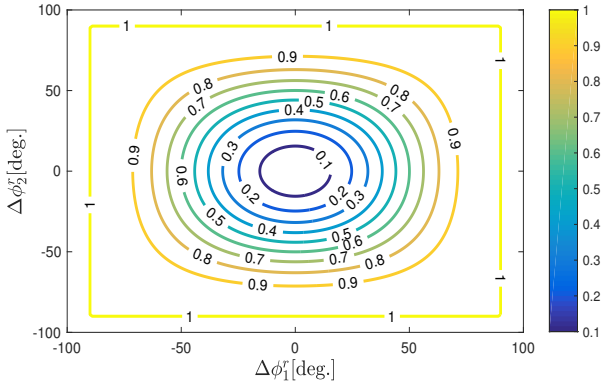

(b) $(\eta_1^r, \eta_2^r) = (0.9, 1.15)$

Fig. 2. Level of impropriety ξ_v of the observed baseband noise as a function of (a) (η_1^r, η_2^r) and (b) $(\Delta\phi_1^r, \Delta\phi_2^r)$ for $M = 2$.

$\xi_v = 0$, while the worst case phase mismatch of $\Delta\phi_m^r = \pi/2$ yields $\xi_v = 1$. In addition, it can be observed that the level of impropriety increases as the number of receive antennas increases since $d_m \leq 1$. Therefore, the multi-antenna receiver configuration is effectively increasing the level of impropriety of the observed baseband noise. In Fig. 2, the impropriety measure ξ_v is visually illustrated as a function of (a) (η_1^r, η_2^r) and (b) $(\Delta\phi_1^r, \Delta\phi_2^r)$ for $M = 2$.

Similarly, we adopt for analysis purposes an assumption that the I/Q impaired transmit signal vector $\mathbf{s}[n]$ is expressible as an improper Gaussian with zero mean, implying thus

$$f(\mathbf{s}[n]) = \frac{1}{\pi^2 |\underline{\mathbf{R}}_s|^{1/2}} \exp\{-\frac{1}{2}\underline{\mathbf{s}}[n]^H \underline{\mathbf{R}}_s^{-1} \underline{\mathbf{s}}[n]\} \tag{27}$$

where $\underline{\mathbf{R}}_s = E\{\underline{\mathbf{s}}[n]\underline{\mathbf{s}}[n]^H\}$ partitions as

$$\underline{\mathbf{R}}_s = \begin{bmatrix} [\underline{\mathbf{R}}_s]_{1,1} & [\underline{\mathbf{R}}_s]_{1,2} \\ [\underline{\mathbf{R}}_s]_{1,2}{}^* & [\underline{\mathbf{R}}_s]_{1,1} \end{bmatrix} \tag{28}$$

By using (12) together with some manipulations, it can be shown that

$$[\underline{\mathbf{R}}_s]_{1,1} = \sigma_s^2[n](|k_1^t|^2 + |k_2^t|^2 + 2\Re\{k_1^t k_2^{t\,*} \rho_p\}), \tag{29}$$

$$[\underline{\mathbf{R}}_s]_{1,2} = \sigma_s^2[n](k_1^{t\,2}\rho_p + 2k_1^t k_2^t + k_2^{t\,2}\rho_p^*) \tag{30}$$

where $\sigma_s^2[n] = E\{|p[n]|^2\}$ while ρ_p denotes the complex correlation coefficient defined as $\rho_p = \frac{E\{p[n]^2\}}{E\{|p[n]|^2\}} = \xi_p e^{\psi_p}$, with $\xi_p \leq 1$. In general, the level of impropriety/noncircularity of the ideal transmit signal $p[n]$ is measured by ξ_p. Specifically, if $\xi_p = 0$, the signal is said to be proper or circular, while if $\xi_p = 1$, the signal is maximally improper or noncircular. For example, the BPSK signal, 8-PSK signal and 8-QAM signal have degrees of impropriety of 1, 0 and $2/3$, respectively [36]. Similarly, for the actual transmitted signal $s[n]$, the complex correlation coefficient ρ_s can be defined as

$$\rho_s = \frac{[\underline{\mathbf{R}}_s]_{12}}{[\underline{\mathbf{R}}_s]_{11}} \tag{31}$$

By substituting now (29) and (30) into (31), we can establish that

$$\rho_s = \frac{k_1^{t\,2}\rho_p + 2k_1^t k_2^t + k_2^{t\,2}\rho_p^*}{|k_1^t|^2 + |k_2^t|^2 + 2\Re\{k_1^t k_2^{t\,*}\rho_p\}} \tag{32}$$

In Fig. (3), the absolute value of ρ_s as a function of η_t and $\Delta\phi_t$ is plotted for both 8-PSK and 8-QAM signals. It is seen that the worst possible TX I/Q imbalance case of $|\eta_t - 1| \approxeq 1$ and $\Delta\phi_t = \pm\pi/2$ result in $|\rho_s| = 1$. From Fig. (3), it is also seen that the improperness on the transmitted signal can be strengthened through the TX I/Q imbalance. For instance, the degree of impropriety of the 8-PSK is equal to 0.4 with TX I/Q imbalances of $\Delta\phi_t = 11^\circ$ and $\eta_t = 0.7$, while it is zero with perfect TX I/Q balance. In this case, the worst possible TX I/Q imbalance results in $\rho_s = 0.9$. Overall, we conclude that an improper transmitted signal arises under TX I/Q imbalance even when the ideal transmitted signal is proper.

B. Proposed Spectrum Sensing Techniques

In what follows, we assume that the primary user modulated waveform $\underline{\mathbf{s}}$ and the observable noise $\underline{\mathbf{v}}[n]$ are mutually independent. As a result, the received augmented signal vector $\underline{\mathbf{y}}[n]$ can be characterized through an improper complex Gaussian distribution with zero mean, i.e., $\underline{\mathbf{y}}[n] \sim \mathcal{CN}(\mathbf{0}, \underline{\mathbf{Q}})$, where

$$\begin{cases} H_0 : \underline{\mathbf{Q}} = \underline{\mathbf{R}}_v, \\ H_1 : \underline{\mathbf{Q}} = \underline{\mathbf{H}}\underline{\mathbf{R}}_s\underline{\mathbf{H}}^H + \underline{\mathbf{R}}_v, \end{cases} \tag{33}$$

To now solve the spectrum sensing problem, we deploy a likelihood ratio test (LRT) based approach to decide whether the primary user signal is absent or present. Based on [38]-[41], we define the LRTs as follows:

Definition 3. *The LRT for testing $H_0 : \theta \in \Theta_0$ versus $H_1 : \theta \in \Theta_0^c$ is*

$$T(\underline{\mathbf{Y}}) = \sup_{\Theta_0}\{\mathcal{L}(\underline{\mathbf{Y}}; \underline{\mathbf{Q}})\} - \sup_{\Theta}\{\mathcal{L}(\underline{\mathbf{Y}}; \underline{\mathbf{Q}})\} \underset{H_1}{\overset{H_0}{\gtrless}} \eta. \tag{34}$$

The first and second parts in the above test statistics refer to the suprema of the log-likelihood function (LLF) of the observation matrix, which are computed for the parameters corresponding to the null hypothesis, denoted as Θ_0, and for the all possible parameters, denoted by $\Theta = \Theta_0 \cup \Theta_0^c$, respectively. η, in turn, refers any non-positive number [41].

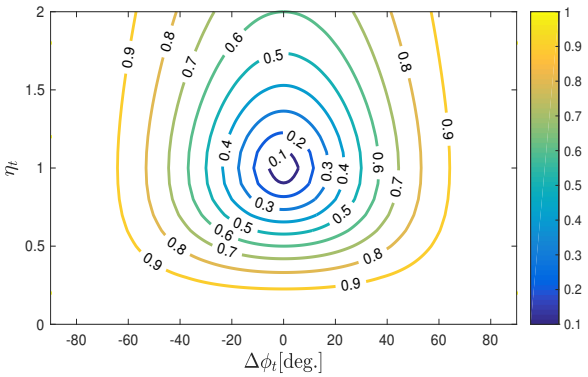

(a) 8-PSK signal with $\rho_p = 0$

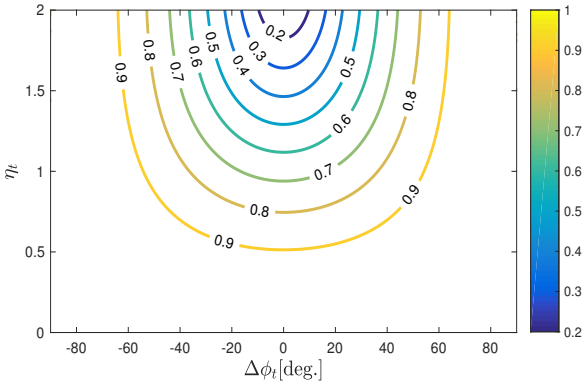

(b) 8-QAM signal with $\rho_p = \frac{2}{3}$

Fig. 3. Level of impropriety ρ_s of the transmitted signal as a function of transmitter amplitude and phase mismatches for different signals.

Next we express the LLF corresponding to N i.i.d. random vectors drawn from the complex Normal distribution expressed as $\mathcal{CN}(\mathbf{0}, \underline{\mathbf{Q}})$. The LLF can be written as

$$\mathcal{L}(\underline{\mathbf{Y}}; \underline{\mathbf{Q}}) = -2MN\ln(\pi) - \frac{N}{2}\ln(|\underline{\mathbf{Q}}|) - \frac{1}{2}\mathrm{tr}\left(\underline{\mathbf{Q}}^{-1}\underline{\mathbf{Y}}\underline{\mathbf{Y}}^H\right), \tag{35}$$

Our previous developments clearly showed that the observed baseband noise and the observed signal term are both improper. However, the fact that these signals are improper does not necessarily imply that it can be utilized to enhance the detection performance of spectrum sensing algorithms. To examine and address this issue systematically, we consider next the following three scenarios or spectrum sensing problems (SSPs):

- **SSP1:** In the first spectrum sensing problem, we take into account the improper nature of both the desired signal and the observable noise to derive a new spectrum sensing algorithm. Thus, in this case, we have $\Theta_0 = \{\underline{\mathbf{R}}_v\}$ where the matrix $\underline{\mathbf{R}}_v$ has block-diagonal structure as shown in (18). Additionally, $\Theta_1 = \{\underline{\mathbf{Q}}\}$ where we do not use any specific structure for the augmented covariance matrix $\underline{\mathbf{Q}}$ under H_1 hypothesis other than it is assumed to be positive definite.
- **SSP2:** In the second spectrum sensing problem, we consider the improper nature of the desired signal while consider the observable noise as proper when deriving the spectrum sensing algorithm. In this case, we have $\Theta_0 = \{\underline{\mathbf{R}}_{v,0}\}$, in which $\{\underline{\mathbf{R}}_{v,0}\}$ is given in (22) and $\Theta_1 = \{\underline{\mathbf{Q}}\}$.
- **SSP3:** In the third spectrum sensing problem, neither the improper nature of the desired signal nor the noise is taken into account when devising the spectrum sensing algorithm. In this case, we have $\Theta_0 = \{\underline{\mathbf{R}}_{v,0}\}$ and $\Theta_1 = \{\underline{\mathbf{Q}}\}$ in which we replace $\underline{\mathbf{R}}_s$ with $\underline{\mathbf{R}}_{s,0} = \mathrm{diag}([\underline{\mathbf{R}}_s]_{1,1}, [\underline{\mathbf{R}}_s]_{1,1})$.

Proposition 1. *The LRT statistic $T(\boldsymbol{Y})$ of the SSP1 can be expressed compactly as*

$$T_1(\boldsymbol{Y}) = \frac{\left|\left[\begin{array}{cc} \frac{1}{2N}\mathrm{Diag}(\boldsymbol{Y}\boldsymbol{Y}^H + \boldsymbol{Y}^*\boldsymbol{Y}^T) & \frac{1}{N}\mathrm{Diag}(\boldsymbol{Y}\boldsymbol{Y}^T) \\ \frac{1}{N}\mathrm{Diag}(\boldsymbol{Y}^*\boldsymbol{Y}^H) & \frac{1}{2N}\mathrm{Diag}(\boldsymbol{Y}\boldsymbol{Y}^H + \boldsymbol{Y}^*\boldsymbol{Y}^T) \end{array}\right]\right|}{\left|\left[\begin{array}{cc} \boldsymbol{Y}\boldsymbol{Y}^H & \boldsymbol{Y}\boldsymbol{Y}^T \\ \boldsymbol{Y}^*\boldsymbol{Y}^H & \boldsymbol{Y}^*\boldsymbol{Y}^T \end{array}\right]\right|}. \tag{36}$$

Proof. The derivation of the above test statistic is given in Appendix A. Let ζ_1 be the decision threshold of the proposed Improper Signal and Improper Noise LRT, abbreviated as IS+IN-LRT. The hypothesis H_1 is accepted if $T_1(\mathbf{Y})$ is greater than ζ_1; otherwise the null hypothesis H_0 is accepted. □

Proposition 2. *The LRT statistic $T(\boldsymbol{Y})$ of the SSP2 has the following compact form*

$$T_2(\boldsymbol{Y}) = \frac{\left|\left[\begin{array}{cc} \frac{1}{2N}\mathrm{Diag}(\boldsymbol{Y}\boldsymbol{Y}^H + \boldsymbol{Y}^*\boldsymbol{Y}^T) & \boldsymbol{0}_{M,M} \\ \boldsymbol{0}_{M,M} & \frac{1}{2N}\mathrm{Diag}(\boldsymbol{Y}\boldsymbol{Y}^H + \boldsymbol{Y}^*\boldsymbol{Y}^T) \end{array}\right]\right|}{\left|\left[\begin{array}{cc} \boldsymbol{Y}\boldsymbol{Y}^H & \boldsymbol{Y}\boldsymbol{Y}^T \\ \boldsymbol{Y}^*\boldsymbol{Y}^H & \boldsymbol{Y}^*\boldsymbol{Y}^T \end{array}\right]\right|}. \tag{37}$$

Proof. This statistic is obtained under the constraint that $\underline{\mathbf{R}}_v$ has zero off-diagonal blocks. Here, ζ_2 is the decision threshold of the proposed Improper Signal and Proper Noise LRT, abbreviated as IS+PN-LRT. □

Proposition 3. *The LRT statistic $T(\boldsymbol{Y})$ of the SSP3 has the following compact form*

$$T_3(\boldsymbol{Y}) = \frac{\left|\left[\begin{array}{cc} \frac{1}{2N}\mathrm{Diag}(\boldsymbol{Y}\boldsymbol{Y}^H + \boldsymbol{Y}^*\boldsymbol{Y}^T) & \boldsymbol{0}_{M,M} \\ \boldsymbol{0}_{M,M} & \frac{1}{2N}\mathrm{Diag}(\boldsymbol{Y}\boldsymbol{Y}^H + \boldsymbol{Y}^*\boldsymbol{Y}^T) \end{array}\right]\right|}{\left|\left[\begin{array}{cc} \boldsymbol{Y}\boldsymbol{Y}^H & \boldsymbol{0}_{M,M} \\ \boldsymbol{0}_{M,M} & \boldsymbol{Y}^*\boldsymbol{Y}^T \end{array}\right]\right|}. \tag{38}$$

Proof. Similarly, this statistic can be obtained from (36) under the constraints that $\underline{\mathbf{R}}_v$ and $\underline{\mathbf{R}}_s$ have zero off-diagonal blocks. In this case, ζ_3 is the detection threshold of the proposed Proper Signal and Proper Noise LRT, abbreviated as PS+PN-LRT. □

Additionally, it is noted that the proposed LRT decision statistics can be rewritten in the following compact form

$$T_i(\underline{\mathbf{Y}}) = \frac{\left|\underline{\mathbf{Y}}\underline{\mathbf{Y}}^H \odot \mathbf{N}_i\right|}{\left|\underline{\mathbf{Y}}\underline{\mathbf{Y}}^H \odot \mathbf{D}_i\right|}, \tag{39}$$

where

$$\mathbf{N}_i = \frac{1}{N}\begin{cases} \begin{bmatrix} \mathrm{Diag}(\mathbf{1}_M) & \mathrm{Diag}(\mathbf{1}_M) \\ \mathrm{Diag}(\mathbf{1}_M) & \mathrm{Diag}(\mathbf{1}_M) \end{bmatrix}, & i=1 \\ \mathbf{I}_{2M\times 2M}. & i=2,3 \end{cases} \tag{40}$$

and

$$\mathbf{D}_i = \begin{cases} \mathbf{1}_{2M\times 2M}, & i=1,2 \\ \begin{bmatrix} \mathbf{1}_{M\times M} & \mathbf{0}_{M\times M} \\ \mathbf{0}_{M\times M} & \mathbf{1}_{M\times M} \end{bmatrix}, & i=3 \end{cases} \tag{41}$$

Remark 1. *We analytically showed that the RX I/Q imbalances can infer improper features in both the desired signal and noise. In such cases, our problem formulation is different from classical spectrum sensing problems in the literature working with proper/ circular noise, e.g., [13], [35] and references therein.*

Remark 2. *From* $[\underline{\mathbf{R}}_v]_{m,m} = 0.5a_{i,m}^r(1+{\eta_m^r}^2)\sigma_m^2$ *for* $m = 1,...,M$*, we can infer that different RX I/Q imbalance parameters across different RF chains result in different diagonal elements of matrix* $\underline{\mathbf{R}}_v$*. Hence, it is unfeasible to assume well-controlled false alarm rate or acceptable detection performance when utilizing classical spectrum sensing algorithms designed under the assumption of* $\mathbf{\Sigma} = \sigma^2\mathbf{I}$ *and radios with zero I/Q imbalance, e.g., [7]- [10], [35] and references therein.*

IV. CFAR Behavior of the Proposed Detectors

In this section, we exploit the principle of invariance to investigate the potential CFAR behavior of the proposed detectors against NVU and receiver I/Q errors. In general, the goal in the invariance theory is to find transformations leaving the considered hypothesis testing problem invariant [29], [42]-[45]. In other words, to prove CFAR behavior, we need to find transformation $\mathbf{G}$ that preserves the distribution family of the data while achieves $T_i(\mathbf{G}\underline{\mathbf{Y}}) = T_i(\underline{\mathbf{Y}})$. These are pursued next.

A. CFAR Behavior Against Noise Variance Uncertainty

To address the potential CFAR properties of the proposed detectors against NVU, let us first define the transformation $\mathbf{G}$ as $\mathbf{G} = \begin{bmatrix} \mathbf{\Sigma}' & \mathbf{0} \\ \mathbf{0} & \mathbf{\Sigma}' \end{bmatrix}$, where $\mathbf{\Sigma}'$ is an unknown diagonal matrix with positive entries. For this transformation and under hypothesis H_0, the distribution of the transformed date $\mathbf{G}\underline{\mathbf{y}}[n]$ is of the form $\mathcal{CN}(\mathbf{0}, \underline{\mathbf{Q}}')$, where

$$\underline{\mathbf{Q}}' = \begin{bmatrix} (\mathbf{k}_1\mathbf{k}_1^H + \mathbf{k}_2\mathbf{k}_2^H)\odot\mathbf{\Sigma}_x & 2\mathbf{k}_1\mathbf{k}_2^T \odot \mathbf{\Sigma}_x \\ 2\mathbf{k}_1^*\mathbf{k}_2^H \odot \mathbf{\Sigma}_x & (\mathbf{k}_1^*\mathbf{k}_1^T + \mathbf{k}_2^*\mathbf{k}_2^T)\odot\mathbf{\Sigma}_x \end{bmatrix} \tag{42}$$

where $\mathbf{\Sigma}_x = \mathbf{\Sigma}'\mathbf{\Sigma}\mathbf{\Sigma}'$ is also a diagonal and unknown matrix. By comparing (17) and (42), we find that the distribution family of the transformed data does not change. In addition, we have

$$T_i(\mathbf{G}\underline{\mathbf{Y}}) = \frac{\left|\mathbf{G}\underline{\mathbf{Y}}\underline{\mathbf{Y}}^H\mathbf{G} \odot \mathbf{N}_i\right|}{\left|\mathbf{G}\underline{\mathbf{Y}}\underline{\mathbf{Y}}^H\mathbf{G} \odot \mathbf{D}_i\right|} \tag{43}$$

For diagonal matrix $\mathbf{G}$ it is easy to show that $\mathbf{G}\underline{\mathbf{Y}}\underline{\mathbf{Y}}^H\mathbf{G}\odot\mathbf{N}_i = \mathbf{G}(\underline{\mathbf{Y}}\underline{\mathbf{Y}}^H \odot \mathbf{N}_i)\mathbf{G}$ and $\mathbf{G}\underline{\mathbf{Y}}\underline{\mathbf{Y}}^H\mathbf{G} \odot \mathbf{D}_i = \mathbf{G}(\underline{\mathbf{Z}}\underline{\mathbf{Y}}^H \odot \mathbf{D}_i)\mathbf{G}$, resulting in $T_i(\mathbf{G}\underline{\mathbf{Y}}) = T_i(\underline{\mathbf{Y}})$ for the proposed detectors. All of these imply that the detection thresholds of the proposed detectors remain constant even when the different noise variances across different RF chains change. Thus, this proves the CFAR behavior against different noise variance uncertainties across the RF chains.

B. CFAR Behavior Against RX I/Q Imbalance Values

To next investigate the CFARness of the proposed methods against RX I/Q imbalance parameters, based on (18), we define the transformation $\mathbf{G}$ as

$$\mathbf{G} = \begin{bmatrix} \mathrm{diag}(\mathbf{e}) & \mathrm{diag}(\mathbf{p}) \\ \mathrm{diag}(\mathbf{p}^*) & \mathrm{diag}(\mathbf{e}) \end{bmatrix} \tag{44}$$

where $\mathbf{e} = [e_1,...,e_M]^T$ and $\mathbf{u} = [p_1,...,p_M]^T$. It is not difficult to show that the transformed data $\mathbf{G}\underline{\mathbf{y}}[n]$ has a same covariance matrix structure as that of (18). Now, we need to check the property $T_i(\mathbf{G}\underline{\mathbf{Y}}) = T_i(\underline{\mathbf{Y}})$ for $i = 1,2,3$, i.e.,

$$\frac{\left|\mathbf{G}\underline{\mathbf{Y}}\underline{\mathbf{Y}}^H\mathbf{G} \odot \mathbf{N}_i\right|}{\left|\mathbf{G}\underline{\mathbf{Y}}\underline{\mathbf{Y}}^H\mathbf{G} \odot \mathbf{D}_i\right|} = \frac{\left|\underline{\mathbf{Y}}\underline{\mathbf{Y}}^H \odot \mathbf{N}_i\right|}{\left|\underline{\mathbf{Y}}\underline{\mathbf{Y}}^H \odot \mathbf{D}_i\right|} \tag{45}$$

For the proposed IS+IN-LRT method, the matrix $\mathbf{G}$ is not a diagonal matrix, however, the structure of matrix $\mathbf{N}_1$ allows us to again get $\mathbf{G}\underline{\mathbf{Y}}\underline{\mathbf{Y}}^H\mathbf{G}\odot\mathbf{N}_1 = \mathbf{G}(\underline{\mathbf{Y}}\underline{\mathbf{Y}}^H\odot\mathbf{N}_1)\mathbf{G}$. Considering this and $\mathbf{G}\underline{\mathbf{Y}}\underline{\mathbf{Y}}^H\mathbf{G} \odot \mathbf{D}_1 = \mathbf{G}\underline{\mathbf{Y}}\underline{\mathbf{Y}}^H\mathbf{G}$ together, we arrive at $T_1(\mathbf{G}\underline{\mathbf{Y}}) = T_1(\underline{\mathbf{Y}})$. This means that the IS+IN-LRT detector has CFAR behavior against the RX I/Q imbalance parameters. Similarly, since $\mathbf{D}_2 = \mathbf{D}_1$ but $\mathbf{N}_2 \neq \mathbf{N}_1$, we arrive at $T_2(\mathbf{G}\underline{\mathbf{Y}}) \neq T_2(\underline{\mathbf{Y}})$, implying that the proposed IS+PN-LRT method does not have CFAR property against the RX I/Q imbalance parameters. Finally, for the PS+PN-LRT method, (45) can be reduced to $\frac{\left|\mathbf{G}'\mathbf{Y}\mathbf{Y}^H\mathbf{G}'\odot\mathbf{I}_{M\times M}\right|^2}{\left|\mathbf{G}'\mathbf{Y}\mathbf{Y}^H\mathbf{G}'\odot\mathbf{1}_{M\times M}\right|^2} = \frac{\left|\mathbf{Y}\mathbf{Y}^H\odot\mathbf{I}_{M\times M}\right|^2}{\left|\mathbf{Y}\mathbf{Y}^H\odot\mathbf{1}_{M\times M}\right|^2}$, where $\mathbf{G}' = \mathrm{diag}(\mathbf{e})$. Here, since the matrix $\mathbf{G}'$ is a diagonal matrix, we get $\mathbf{G}'\mathbf{Y}\mathbf{Y}^H\mathbf{G}'\odot\mathbf{I}_{M\times M} = \mathbf{G}'(\mathbf{Y}\mathbf{Y}^H\odot\mathbf{I}_{M\times M})\mathbf{G}'$ and $\mathbf{G}'\mathbf{Y}\mathbf{Y}^H\mathbf{G}'\odot\mathbf{1}_{M\times M} = \mathbf{G}'(\mathbf{Y}\mathbf{Y}^H\odot\mathbf{1}_{M\times M})\mathbf{G}'$, resulting in $T_3(\mathbf{G}'\mathbf{Y}) = T_3(\mathbf{Y})$. This completes the proof of the CFAR property of the PS+PN-LRT detector against RX I/Q imbalance values.

V. Numerical Results and Analysis

Next, we assess the achievable spectrum sensing performance of the proposed methods in different numerical evaluation cases. Firstly, we address the issue of setting the detection thresholds, in different detector and RX I/Q imbalance cases, in order to reach the target false alarm probability p_{fa}. Then, the results of the selected simulation cases are presented and analyzed, to demonstrate the sensing performance that the proposed detectors can offer and to obtain technical insight whether to use proper or improper nature of the desired signal and noise. Additionally, comparisons against known state-of-the-art reference methods are presented.

TABLE I
CONSIDERED RECEIVER RF CHAIN CHARACTERISTICS

Case	A	B
Number of antennas	4	8
per-antenna noise variances σ_m^2	(1,-1.7,-0.75,0.5) dB	(0,-1,1,0.5,-2,-0.3,0.75,0.25) dB
I branch amplitudes $a_{i,m}^r$	(-1,0,1,2) dB	(-2,0,1,2,-0.75,0.5,1.2,0.25) dB
Amplitude mismatches η_m^r	(1.1,1.2,1.03,0.9)	(0.9,1.5,1.3,1.4,1.1,0.89,1.2,0.8)
Phase mismatches $\Delta\phi_m^r$ [deg.]	(-1,-3,-5,10)	(-10,-3,-5,-6,1,0,2,9)

A. False-Alarm Probability Versus Threshold

The false alarm probabilities versus the detection threshold are evaluated and plotted in Fig. 4 for two different numbers of receiver antennas and when $N = 500$. The detector thresholds are determined by 10^5 Monte-Carlo (MC) simulation runs to assure the reliability of the results. In Fig. 4, two fundamental scerios are addressed, namely (1) the so-called ideal RX (IRX) case where all receivers have perfect I/Q balance and identical noise variance across the receiver chains, and (2) the practical RF receiver case with parameters reported in Table I. From Fig. 4, it is seen that the IS+IN-LRT and PS+PN-LRT detectors have the CFAR characteristic with respect to receiver I/Q error parameters as well as different noise variances across different RF chains, while the IS+PN-LRT detector does not posses the CFAR property against the RX I/Q imbalance parameters. Thus, the obtained numerical results confirm our analytical CFAR conclusions obtained in Section IV.

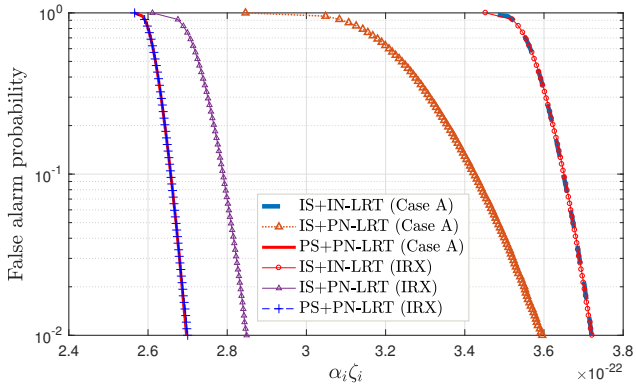

(a) $M = 4$ and $N = 500$

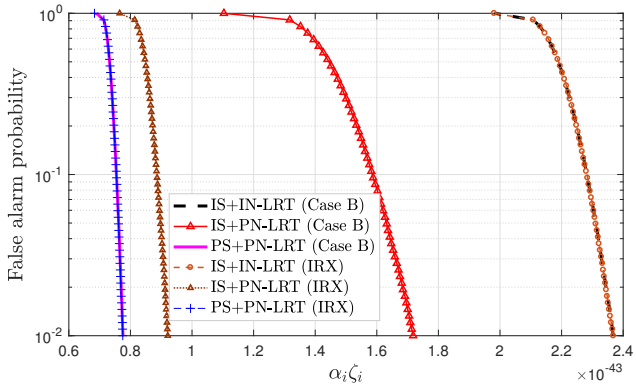

(b) $M = 8$ and $N = 500$

Fig. 4. Monte-Carlo false alarm probabilities as functions of detection thresholds $\frac{\zeta_1}{6N}$ (i.e., $\alpha_1 = \frac{1}{6N}$), ζ_2 (i.e., $\alpha_2 = 1$) and ζ_3 (i.e., $\alpha_3 = 1$) for the proposed detectors for two scenarios; (1) ideal RX (IRX) with perfect RX I/Q balance and identical noise variance across receiver chains, (2) practical RF receivers with parameters reported in Table I.

B. Detection Probability Versus SNR

Fig. 5 depicts the corresponding detection probabilities of the different detectors versus SNR at target $p_{fa} = 0.01$, $M = 4$, and $N = 500$, when the primary user utilizes (a) a BPSK modulation, (b) an 8-QAM modulation, and (c) an 8-PSK modulation. Moreover, for each modulation case, two alternative values of the TX I/Q imbalance parameters $(a_i^t, \eta_t, \phi_t, \Delta\phi_t)$ are evaluated, namely $(1, 0.85, 2, -10)$ and $(1, 1.15, -2, 7)$. The receiver assumptions follow the "case A" defined in Table I. The resulting detection thresholds of the proposed alternative detection methods are equal to $\zeta_1 = 11.160 \times 10^{-19}$, $\zeta_2 = 3.596 \times 10^{-22}$ and $\zeta_3 = 2.697 \times 10^{-22}$. A classical Rayleigh fading assumption is adopted for the PU-SU array channel $\mathbf{h}$ such that independent realizations are randomly generated from zero-mean complex Normal distribution for the different simulation runs while the channel is assumed to be fixed during an individual sensing window. The input signal-to-noise ratio averaged across the receivers is set according to

$$\text{SNR}_i = \frac{P}{\frac{1}{M}\sum_{m=1}^{M}\sigma_m^2} \tag{46}$$

where $P = \frac{1}{N}E(||\mathbf{p}||_2^2)$ is referred to as the transmitted power.

From Fig. 5, we can observe the following. For the BPSK signal with the maximal impropriety, the detection performance of the proposed methods does not depend on the I/Q imbalance level of the PU transmitter. Furthermore, the detection performance of the IS+IN-LRT is the highest, while that of the IS+PN-LRT is ca. 1 dB lower being finally followed by the PS+PN-LRT detector which performs the worst. For the 8-QAM signal, in turn, with the impropriety degree of $\frac{2}{3}$, the detection performances of the IS+IN-LRT and PS+PN-LRT are very similar, while the IS+PN-LRT detector is clearly performing weaker. These observations apply to both $\eta_t = 0.85$ for which $\rho_s = 0.756$ and $\eta_t = 1.25$ for which $\rho_s = 0.534$. The exact though relatively small differences between the different η_t cases are mainly due to the fact that the value of amplitude mismatches less than one can strengthen the impropriety degree of the transmitted signal (see Fig. 2). For the 8-PSK signal with the maximal propriety, the detection performance of the PS+PN-LRT is the best being then followed by the IS+IN-LRT and IS+PN-LRT. For the latter two, the levels of impropriety are equal to 0.235 and 0.249 for $\eta_t = 0.85$ and $\eta_t = 1.25$, respectively. The same

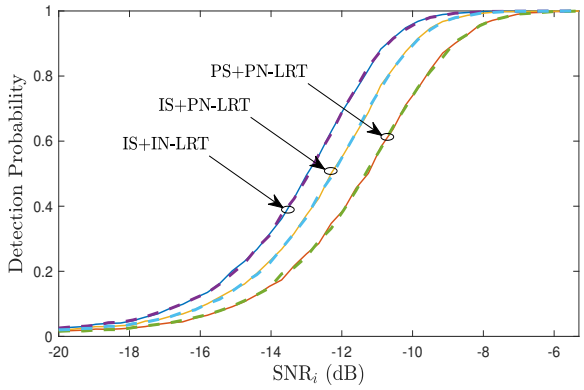

(a) BPSK PU signal

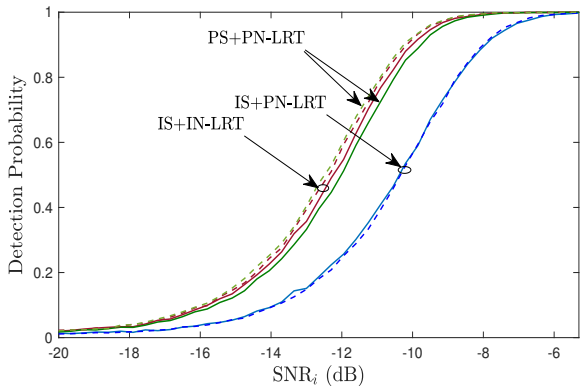

(b) 8-QAM PU signal

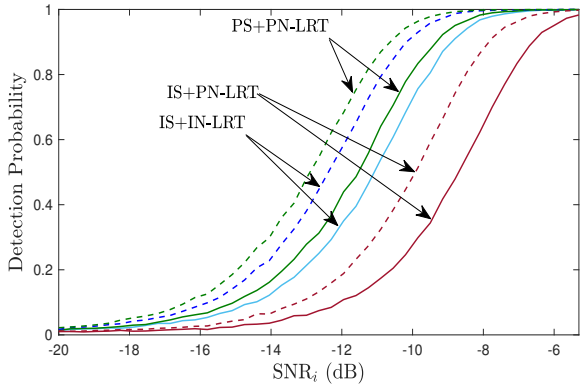

(c) 8-PSK PU signal

Fig. 5. Detection probabilities versus input SNR for three proposed detectors at $p_{fa} = 0.01$, $M = 4$, $N = 500$ for three different PU modulation types. The receiver assumptions follow the case A defined in Table I. The solid lines correspond to $(a_i^t, \eta_t, \phi_t, \Delta\phi_t) = (1, 0.85, 2, -10)$, while the dashed lines correspond to $(a_i^t, \eta_t, \phi_t, \Delta\phi_t) = (1, 1.15, -2, 7)$.

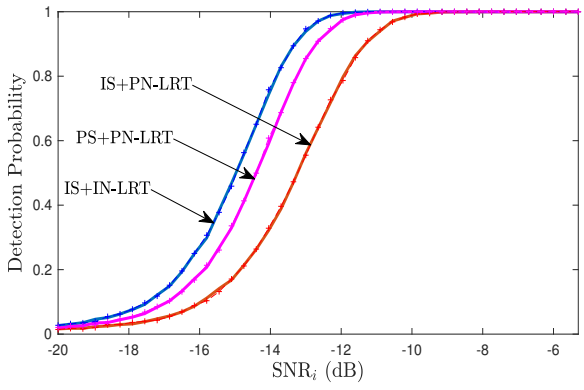

(a) BPSK PU signal

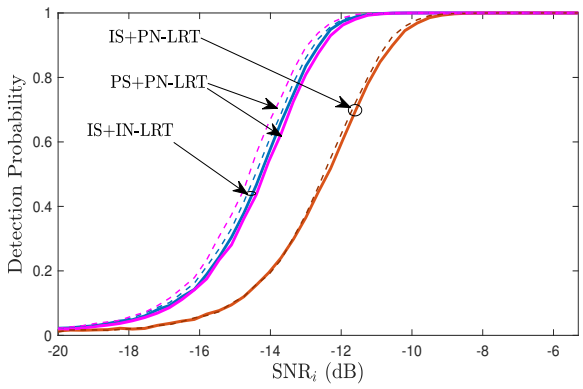

(b) 8-QAM PU signal

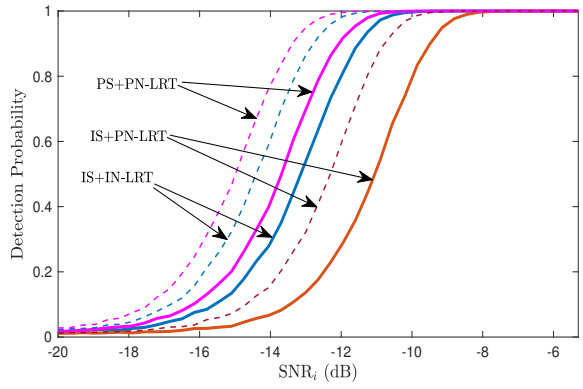

(c) 8-PSK PU signal

Fig. 6. Detection probabilities versus input SNR for three proposed detectors at $p_{fa} = 0.01$, $M = 8$, $N = 500$ for three different PU modulation types. The receiver assumptions follow the case B defined in Table I. The solid lines correspond to $(a_i^t, \eta_t, \phi_t, \Delta\phi_t) = (1, 0.85, 2, -10)$, while dashed lines correspond to $(a_i^t, \eta_t, \phi_t, \Delta\phi_t) = (1, 1.15, -2, 7)$.

performance assessment is also carried out for $M = 8$ and the corresponding results are shown in Fig. 6, where the receiver assumptions correspond to the "case B" defined in Table I. As can be seen, very similar trends can be observed for $M = 8$ compared to those in Fig. 5 and thus the conclusions are to many extent similar. Additionally, by comparing the results of these figures, we can observe that by increasing the number of receive antennas, the detection performance of the proposed detectors can also be improved accordingly.

Next, to obtain and provide further insight into the TX and RX radio I/Q imbalance levels, we examine and derive the effective received SNR, defined as

$$\text{SNR}_r = \frac{E\left(||\mathbf{HS}||_F^2\right)}{E\left(||\mathbf{V}||_F^2\right)}. \tag{47}$$

Through straight-forward manipulations, this can be written as

$$\text{SNR}_r = \frac{E\{\mathbf{p}^H\mathbf{p}\}}{N\sum_{m=1}^{M}\sigma_m^2}(|k_1^t|^2 + |k_2^t|^2 + 2\Re\{k_1^{t\,*}k_2^t\rho_p\}) \times (E\{\mathbf{h}^H\mathbf{h}\}\odot\mathbf{k}_1^H\mathbf{k}_1 + E\{\mathbf{h}^T\mathbf{h}^*\}\odot\mathbf{k}_2^H\mathbf{k}_2) \quad (48)$$

In (48), we have used the fact that the array channel $\mathbf{h}$ and the actual transmitted signal vector $\mathbf{s}$ are uncorrelated as well as $\mathbf{v}[n] \sim \mathcal{CN}(\mathbf{0}, \mathbf{\Sigma})$. Assuming again Rayleigh fading where $\mathbf{h} \sim \mathcal{CN}(0, \mathbf{I}_M)$, it can be shown that

$$\text{SNR}_r = \text{SNR}_i \times \text{SF}_t \times \text{SF}_r \quad (49)$$

where the transmit and receive SNR factors (SFs) denoted as SF_t and SF_r, respectively, can be expressed as

$$\text{SF}_t = 0.5(1+\eta_t^2) + \Re\{0.5a_i^{t\,2}\rho_p(1 - 2j\eta_t\sin(\Delta\phi_t) - \eta_t^2)\} \quad (50)$$

$$\text{SF}_r = \sum_{m=1}^{M} 0.5a^{r\,2}_{i,m}(1+\eta_m^{r\,2}) \quad (51)$$

For reference, in the case of perfect TX and RX, we get $\text{SF}_t = 1$ and $\text{SF}_r = M$. As expected, SF_t depends on amplitude mismatch η_t, phase mismatch $\Delta\phi_t$, I channel amplitude a_i^t and the level of impropriety of the ideal transmitted signal $\mathbf{p}$. For proper signals with $\rho_p = 0$, we have $\text{SF}_t = 0.5(1+\eta_t^2)$. This means that by increasing η_t the receive SNR is also increased, resulting in some detection performance improvements, cf. Figs. 5(c) and 6(c). When ρ_p is real-valued, we obtain $\text{SF}_t = 0.5\left(1 + (1 - a_i^{t\,2}\rho_p)\eta_t^2 + a_i^{t\,2}\rho_p\right)$. In the case of maximally improper signal with $\rho_p = 1$, we get $\text{SF}_t = 0.5\left(1 + (1 - a_i^{t\,2})\eta_t^2 + a_i^{t\,2}\right)$, resulting into $\text{SF}_t = 1$ for $a_i^t = 1$; otherwise it depends on η_t. In Fig. 7, the behavior of SF_t is plotted as a function of η_t for different values of a_i^t, for both BPSK and 8-QAM signal types. We observe that by increasing η_t, the SF_t is increased for 8-QAM signal (and 8-PSK), while it is decreased for BPSK signal.

C. Detection Probability Versus Level of Impropriety

In order to further assess the effects of the impropriety degree of the ideal PU transmit signal on the detection performance, we define a general model [24] of the form

$$\mathbf{p} = \sqrt{1-\kappa_p^2}\mathbf{p}_r + j\kappa_p\mathbf{p}_i \quad (52)$$

where $\mathbf{p}_r$ and $\mathbf{p}_i$ are two uncorrelated real-valued vectors both drawn from $\mathcal{N}(0, \mathbf{I}_N)$. By changing the value of $\kappa_p \in [0,1]$, we can directly control the level of impropriety of the vector $\mathbf{p}$. As shown in Fig.8, the vector $\mathbf{p}$ becomes proper for $\kappa_p = \frac{1}{\sqrt{2}}$, while it is maximally improper for both $\kappa_p = 0$ and $\kappa_p = 1$. Fig. 9 shows then the detection probability versus the level of the impropriety ξ_p at $p_{fa} = 0.01$, $M = 4$ and $N = 500$ for the three proposed detectors and with TX I/Q imbalance parameters of $(\eta_t, \Delta\phi_t) = (0.85, -10)$. The shown numerical values are obtained through averaging over 10^4 independent runs. In this figure, the corresponding results of using the BPSK, 8-QAM, and 8-PSK are also shown for comparison purposes. First, it is seen that the detection probabilities with

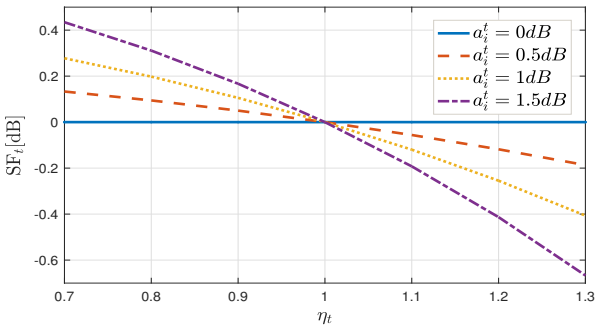

(a) BPSK signal

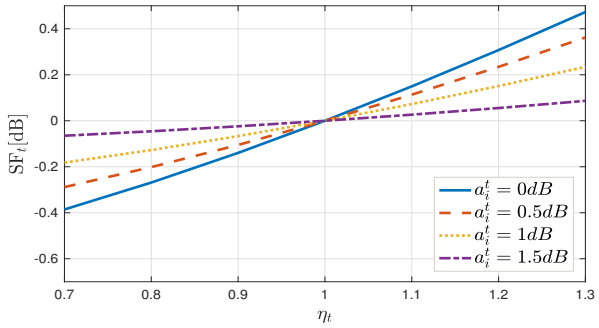

(b) 8-QAM signal

Fig. 7. SF_t as a function of η_t for different values of a_i^t.

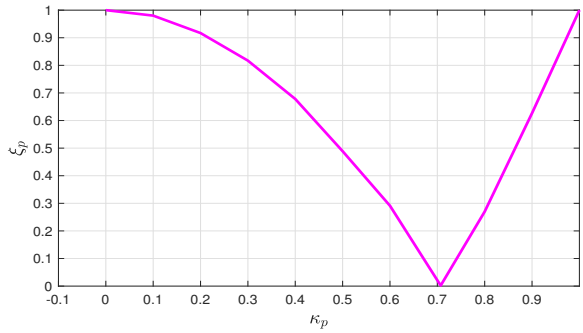

Fig. 8. ξ_p versus κ_p of the general improper signal model (52).

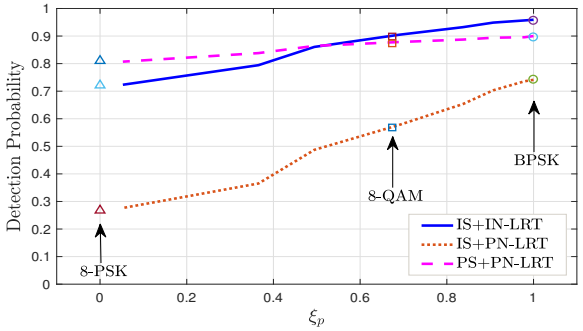

Fig. 9. Detection probabilities of the proposed detectors versus degree of impropriety ξ_p at $p_{fa} = 0.01$ for SNR_i=-10dB.

actual modulated signals are very similar to those of the general improper signal model in (52), as long as the levels of impropriety are also simlar. Second, as can be seen from this figure, for $\xi_p > 0.5$ the IS+IN-LRT detector outperforms the others, while the PS+PN-LRT detector performs better for $\xi_p < 0.5$. As a result, we see that for $\xi_p < 0.5$ the use of the fully improper detector (IS+IN-LRT) is unnecessary and will not improve performance, and thus the fully proper detector (PS+PN-LRT) may be preferable. Otherwise, the IS+IN-LRT detector is preferable.

D. Comparison with Existing Multiantenna Spectrum Sensing Methods

Finally, we pursue and provide performance comparisons of the proposed methods against well-established state-of-the-art reference techniques in the spectrum sensing field. Specifically, we analyze and compare the performance of the proposed detectors with those of the eigenvalue moment ratio (EMR) method [9], the separating function estimation test (SFET)-based method [10], seminal John's method [34] and the volume-based (VB) method [35]. In these numerical evaluations, we again assume $M = 4$, $N = 500$ and consider realistic TX I/Q imbalance parameter values of $(\eta_t, \Delta\phi_t) = (0.85, -10)$. Additionally, the receiver characteristics follow the "case A" defined in Table I. Figs. 10 and 11 depict the Receiver Operating Characteristics (ROC) curves of all the detectors at input SNR of $\text{SNR}_i = -10$ dB, obtained through extensive Monte-Carlo simulations, corresponding to the maximally improper signal ($\kappa_p = 1$) and purely proper signal ($\kappa_p = \frac{1}{\sqrt{2}}$), respectively. From Fig. 10, corresponding to the case of maximally improper signal, it can be seen that the proposed IS+IN-LRT detector performs clearly better than the other detectors, being followed in performance by the PS+PN-LRT, VB, IS+PN-LRT, John's, SFET and EMR detectors. As acknowledged already in Remarks 1 and 2, we see a clear performance degradation of the existing detectors, particularly those that are devised for proper/circular noise and when a calibrated or uncalibrated multi-antenna receiver is assumed. In contract, with purely proper signal, as shown in Fig. 11, the detection performance of the PS+PN-LRT method is the best, being followed by those of the VB, IS+IN-LRT, IS+PN-LRT, John's, SFET and EMR methods.

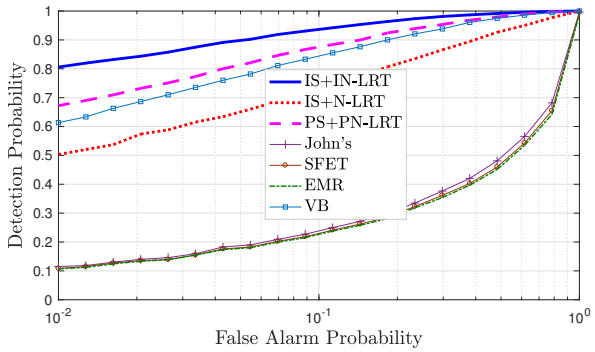

Fig. 10. ROC curves of the proposed detectors and that of the John's, SFET, EMR and VB ones for $M = 4$, $N = 500$, $\kappa_p = 1$, $\text{SNR}_i = -10$dB and when the sensing receiver assumptions follow the case A defined in Table I.

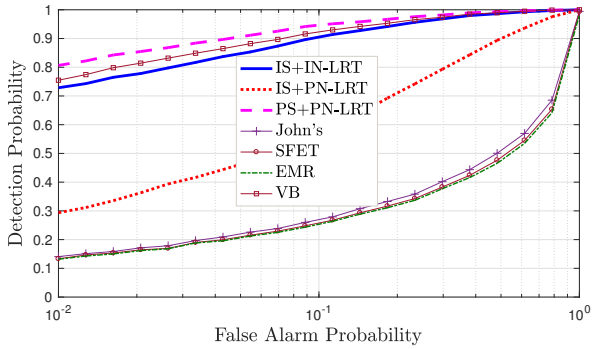

Fig. 11. ROC curves of the proposed detectors and that of the John's, SFET, EMR and VB ones for $M = 4$, $N = 500$, $\kappa_p = \frac{1}{\sqrt{2}}$, $\text{SNR}_i = -10$dB and when the sensing receiver assumptions follow the case A defined in Table I.

VI. Conclusions

This article addressed the SIMO spectrum sensing task and problem in a practical scenario where all the involved radios suffer from I/Q imbalances. To do this, firstly, we modelled the effect of I/Q imbalances on the actual transmitted signal as well as the observed PU signal and noise components in the sensing receiver. We analytically quantified the level of impropriety the involved signal and noise terms as a function of the transmitter and receiver I/Q amplitude and phase uncertainties. Then, the spectrum sensing problem was formulated and solved through the likelihood ratio test (LRT) approach, resulting in three alternative spectrum sensing algorithms based on different assumptions about the impropriety/propriety of the desired and noise signals. Additionally, through the invariance theory, we investigated the potential CFAR behavior of the proposed detectors against noise variance uncertainty as well as the receiver I/Q mismatch characteristics. Specifically, it was shown that all proposed detectors are robust against the noise variance uncertainty, while two out of the three detectors are also robust against RX I/Q imbalance levels. Finally, extensive numerical results were provided to demonstrate and quantify the spectrum sensing performance of the formulated detectors. The obtained results show that it is not necessary to take into account the improper nature of the received signal when the degree of impropriety is small. However, if the underlying signal modulations are already improper, such as 8-QAM or BPSK, much can be gained in the performance if the impropriety of desired signal and noise are taken properly into account in devising the spectrum sensing algorithms. We also derived a closed-form analytical formula for the effective received SNR, expressed as a function of the TX and RX I/Q imbalance values, to quantify and provide further insight on the improvement/degradation in the detection performance that the I/Q imbalances of the involved radios can infer. Finally, performance comparisons against existing spectrum sensing methods were reported, showing particularly the benefits of the proposed IS+IN-LRT detector when the level of the

improperness is large.

APPENDIX A
LRT DERIVATION FOR SSP1

For the first spectrum sensing problem (SSP1), the test statistic is given by

$$T_1(\mathbf{Y}) = \sup_{\underline{\mathbf{R}}_v}\{\mathcal{L}(\underline{\mathbf{Y}};\underline{\mathbf{R}}_v)\} - \sup_{\Theta}\{\mathcal{L}(\underline{\mathbf{Y}};\underline{\mathbf{Q}})\} \tag{53}$$

Using (35), the first part of the expression for $T_1(\mathbf{Y})$ can be written as

$$\begin{aligned}\sup_{\underline{\mathbf{R}}_v}\{\mathcal{L}(\underline{\mathbf{Y}};\underline{\mathbf{R}}_v)\} = \sup_{\underline{\mathbf{R}}_v}\{&-2MN\ln(\pi) - \frac{N}{2}\ln(|\underline{\mathbf{R}}_v|) \\ &- \frac{1}{2}\mathrm{tr}\left({\underline{\mathbf{R}}_v}^{-1}\underline{\mathbf{Y}}\underline{\mathbf{Y}}^H\right)\},\end{aligned} \tag{54}$$

Let us then define and denote the inverse of $\underline{\mathbf{R}}_v$ by $\underline{\mathbf{\Psi}}$, expressed as

$$\underline{\mathbf{\Psi}} = \begin{bmatrix} \mathrm{diag}(\mathbf{a}) & \mathrm{diag}(\mathbf{b}) \\ \mathrm{diag}(\mathbf{b}^*) & \mathrm{diag}(\mathbf{a}) \end{bmatrix} \tag{55}$$

where $\mathbf{a} = [a_1, ..., a_M]^T$ and $\mathbf{b} = [b_1, ..., b_M]^T$. By using

$$\begin{bmatrix} \mathbf{A} & \mathbf{B} \\ \mathbf{C} & \mathbf{D} \end{bmatrix}^{-1} = \begin{bmatrix} \mathbf{A}^{\#} & \mathbf{B}^{\#} \\ \mathbf{C}^{\#} & \mathbf{D}^{\#} \end{bmatrix} \tag{56}$$

where

$$\mathbf{A}^{\#} = (\mathbf{A} - \mathbf{B}\mathbf{D}^{-1}\mathbf{C})^{-1}, \tag{57a}$$
$$\mathbf{B}^{\#} = -(\mathbf{A} - \mathbf{B}\mathbf{D}^{-1}\mathbf{C})^{-1}\mathbf{B}\mathbf{D}^{-1}, \tag{57b}$$
$$\mathbf{C}^{\#} = -\mathbf{D}^{-1}\mathbf{C}(\mathbf{A} - \mathbf{B}\mathbf{D}^{-1}\mathbf{C})^{-1}, \tag{57c}$$
$$\mathbf{D}^{\#} = \mathbf{D}^{-1} + \mathbf{D}^{-1}\mathbf{C}(\mathbf{A} - \mathbf{B}\mathbf{D}^{-1}\mathbf{C})^{-1}\mathbf{B}\mathbf{D}^{-1}, \tag{57d}$$

the relationships between the elements of $\underline{\mathbf{\Psi}}$ and $\underline{\mathbf{R}}_v$ in (18) can be expressed as

$$\begin{aligned} z_m &= [(\mathrm{diag}(\mathbf{a}) - \mathrm{diag}(\mathbf{b})\mathrm{diag}(\mathbf{a})^{-1}\mathrm{diag}(\mathbf{b}^*)^{-1}]_{m,m} \\ &= \frac{a_m}{a_m^2 - b_m b_m^*} \end{aligned} \tag{58}$$

$$\begin{aligned} u_m &= [(\mathrm{diag}(\mathbf{a}) - \mathrm{diag}(\mathbf{b})\mathrm{diag}(\mathbf{a})^{-1}\mathrm{diag}(\mathbf{b}^*)^{-1}]_{m,M+m} \\ &= -\frac{b_m}{a_m^2 - b_m b_m^*} \end{aligned} \tag{59}$$

Instead of directly calculating (54), it is more convenient to work with

$$\begin{aligned}\sup_{\underline{\mathbf{\Psi}}}\{\mathcal{L}(\underline{\mathbf{Y}};\underline{\mathbf{\Psi}})\} = \sup_{\underline{\mathbf{\Psi}}}\{&-2MN\ln(\pi) + \frac{N}{2}\ln(|\underline{\mathbf{\Psi}}|) \\ &- \frac{1}{2}\mathrm{tr}\left(\underline{\mathbf{\Psi}}\underline{\mathbf{Y}}\underline{\mathbf{Y}}^H\right)\}\end{aligned} \tag{60}$$

Thus, we need to obtain $|\underline{\mathbf{\Psi}}|$ and $\mathrm{tr}\left(\underline{\mathbf{\Psi}}\underline{\mathbf{Y}}\underline{\mathbf{Y}}^H\right)$. Using (23) and after some algebraic manipulations, we get

$$|\underline{\mathbf{\Psi}}| = \prod_{m=1}^{M}(a_m^2 - b_m b_m^*), \tag{61}$$

and

$$\begin{aligned}\mathrm{tr}\left(\underline{\mathbf{\Psi}}\underline{\mathbf{Y}}\underline{\mathbf{Y}}^H\right) = &\sum_{m=1}^{M} a_m[\mathbf{Y}\mathbf{Y}^H + \mathbf{Y}^*\mathbf{Y}^T]_{m,m} \\ &+ \sum_{m=1}^{M} b_m[\mathbf{Y}^*\mathbf{Y}^H]_{m,m} \\ &+ \sum_{m=1}^{M} b_m^*[\mathbf{Y}\mathbf{Y}^T]_{m,m}.\end{aligned} \tag{62}$$

Thus, we obtain

$$\begin{aligned}\sup_{\underline{\mathbf{\Psi}}}\{\mathcal{L}(\underline{\mathbf{Y}};\underline{\mathbf{\Psi}})\} = \sup_{\mathbf{a},\mathbf{b}}\{&-2MN\ln(\pi) + \frac{N}{2}\sum_{m=1}^{M}\ln\left(a_m^2 - b_m b_m^*\right) \\ &- \frac{1}{2}\sum_{m=1}^{M} a_m[\mathbf{Y}\mathbf{Y}^H + \mathbf{Y}^*\mathbf{Y}^T]_{m,m} \\ &- \frac{1}{2}\sum_{m=1}^{M} b_m[\mathbf{Y}^*\mathbf{Y}^H]_{m,m} \\ &- \frac{1}{2}\sum_{m=1}^{M} b_m^*[\mathbf{Y}\mathbf{Y}^T]_{m,m}\}.\end{aligned} \tag{63}$$

Now, we must determine which vectors $\mathbf{a}$ and $\mathbf{b}$ maximize the log-likelihood function (LLF). Taking the gradients of the LLF w.r.t the element of vectors $\mathbf{a}$ and $\mathbf{b}$ yields

$$\frac{\partial\mathcal{L}(\underline{\mathbf{Y}};\mathbf{a},\mathbf{b})}{\partial a_m} = \frac{N}{2}\frac{2a_m}{a_m^2 - b_m b_m^*} - \frac{1}{2}[\mathbf{Y}\mathbf{Y}^H + \mathbf{Y}^*\mathbf{Y}^T]_{m,m} \tag{64}$$

$$\frac{\partial\mathcal{L}(\underline{\mathbf{Y}};\mathbf{a},\mathbf{b})}{\partial b_m} = -\frac{N}{2}\frac{b_m^*}{a_m^2 - b_m b_m^*} - \frac{1}{2}[\mathbf{Y}^*\mathbf{Y}^H]_{m,m} \tag{65}$$

Setting the gradients equal to zero and after using (58) and (59) we obtain

$$\hat{z}_m = \frac{1}{N}[\mathbf{Y}\mathbf{Y}^H + \mathbf{Y}^*\mathbf{Y}^T]_{m,m} \tag{66}$$

$$\hat{u}_m = \frac{1}{N}[\mathbf{Y}^*\mathbf{Y}^H]_{m,m} \tag{67}$$

It then follows from (66), (67) and (18) that

$$\underline{\hat{\mathbf{R}}}_v = \begin{bmatrix} \frac{1}{2N}\mathrm{Diag}(\mathbf{Y}\mathbf{Y}^H + \mathbf{Y}^*\mathbf{Y}^T) & \frac{1}{N}\mathrm{Diag}(\mathbf{Y}\mathbf{Y}^T) \\ \frac{1}{2N}\mathrm{Diag}(\mathbf{Y}^*\mathbf{Y}^H) & \frac{1}{2N}\mathrm{Diag}(\mathbf{Y}\mathbf{Y}^H + \mathbf{Y}^*\mathbf{Y}^T) \end{bmatrix} \tag{68}$$

By substituting (66) and (67) into (63), using (61) and after straight-forward manipulations, the first part of (53) can be expressed as

$$\sup_{\underline{\mathbf{R}}_v}\{\mathcal{L}(\underline{\mathbf{Y}};\underline{\mathbf{R}}_v)\} = -2MN\ln(\pi) - \frac{N}{2}\ln(|\underline{\hat{\mathbf{R}}}_v|) - NM \tag{69}$$

Following similar analysis steps and derivations, the second part of (53) can be written as

$$\begin{aligned}\sup_{\underline{\mathbf{Q}}}\{\mathcal{L}(\underline{\mathbf{Y}};\underline{\mathbf{Q}})\} &= -2MN\ln(\pi) - \frac{N}{2}\ln(|\underline{\mathbf{Q}}|) \\ &\quad - \frac{1}{2}\mathrm{tr}\left(\underline{\mathbf{Q}}^{-1}\underline{\mathbf{Y}}\underline{\mathbf{Y}}^{H}\right) \\ &= -2MN\ln(\pi) - \frac{N}{2}\ln(\frac{|\underline{\mathbf{Y}}\underline{\mathbf{Y}}^{H}|}{2MN}) - MN \end{aligned} \tag{70}$$

Substituting (69) and (70) into (53) and after some algebraic manipulations, the proof is completed.

REFERENCES

[1] L. Zhang, M. Xiao, G. Wu, M. Alam, Y.-C. Liang, and S. Li, "A survey of advanced techniques for spectrum sharing in 5G networks" *IEEE Wireless Communications*, vol. 24, no. 5,pp.44-51, 2017.

[2] F. Hu, B. Chen and K. Zhu, "Full spectrum sharing in cognitive radio networks toward 5G: A survey", *IEEE Access*, vol. 6, no. 1, pp. 15754 - 15776, February 2018.

[3] E. Axell, G. Leus, E. G. Larsson and H. V. Poor, "Spectrum Sensing for Cognitive Radio : State-of-the-Art and Recent Advances," *IEEE Signal Processing Mag.* , vol. 29, no. 3, pp. 101-116, May 2012.

[4] T. M. Getu, W. Ajib, and R. Landry, "Simple-F-test-based spectrum sensing techniques for multi-antenna cognitive radios, *IEEE Trans. Commun.*, vol. 66, no. 11, pp. 50815096, Nov. 2018.

[5] L. Lv, J. Chen, Q. Ni, Z. Ding, and H. Jiang, "Cognitive Non-Orthogonal Multiple Access with Cooperative Relaying: A New Wireless Frontier for 5G Spectrum Sharing", arXiv preprint arXiv:1801.04022, 2018.

[6] X. Wang, S. Ekin and E. Serpedin, "Joint Spectrum Sensing and Resource Allocation in Multi-Band-Multi-User Cognitive Radio Networks", *IEEE Trans. Commun.*, DOI 10.1109/TCOMM.2018.2807432.

[7] A. Taherpour, M. Nasiri-Kenari and S. Gazor, "Multiple Antenna Spectrum Sensing in Cognitive Radios," *IEEE Trans. Wireless Commun.*, vol. 9, no. 2, pp. 814-823, February 2010.

[8] Y. Zeng and Y. C. Liang, "Eigenvalue-based Spectrum Sensing Algorithms for Cognitive Radio," *IEEE Trans. Commun.* , vol. 57, no. 6, pp. 1784-1793, June 2009.

[9] L. Huang, J. Fang, K. Liu, H. C. So and H. Li, "An Eigenvalue-Moment-Ratio Approach to Blind Spectrum Sensing for Cognitive Radio Under Sample-Starving Environment," *IEEE Trans. Veh. Technol.*, vol. 64, no. 8, pp. 3465-3480, Aug. 2015.

[10] S. Sedighi, A. Taherpour, S. Gazor and T. Khattab, "Eigenvalue-Based Multiple Antenna Spectrum Sensing: Higher Order Moments," *IEEE Trans. Wireless Commun.* , vol. 16, no. 2, pp. 1168-1184, Feb. 2017.

[11] L. Huang, Y. Xiao, H. C. So and J. Fang, "Accurate Performance Analysis of Hadamard Ratio Test for Robust Spectrum Sensing," *IEEE Trans. Wireless Commun.* , vol. 14, no. 2, pp. 750-758, Feb. 2015.,

[12] A. Zaimbashi, "Spectrum Sensing of MIMO SC-FDMA Signals in Cognitive Radio Networks: UMP-Invariant Test", in *Proc. International Conference in New Research in Electrical Engineering and Computer Science*, Ramsar, Iran, May 2016.

[13] L. Huang, Y. H. Xiao and Q. T. Zhang, "Robust Spectrum Sensing for Noncircular Signal in Multiantenna Cognitive Receivers," *IEEE Trans. Signal Process.*, vol. 63, no. 2, pp. 498-511, Jan.15, 2015.

[14] A. Patel, H. Ram, A. K. Jagannatham, and P. K. Varshney, "Robust cooperative spectrum sensing for MIMO cognitive radio networks under CSI uncertainty," *IEEE Trans. Signal Process.*, vol. 66, no. 1, pp. 1833, 2018.

[15] B. Razavi, *RF Microelectronics*, 2nd ed. Upper Saddle River, NJ: Prentice Hall, 2011.

[16] M. Valkama, M. Renfors, and V. Koivunen, "Compensation of frequencySelective I/Q imbalances in wideband receivers: Models and algorithms, in *Proc. 3rd IEEE Workshop Signal Processing Advances Wireless Communications (SPAWC)*, Taiwan, Mar. 2001, pp. 42-45.

[17] M. Valkama, M. Renfors and V. Koivunen, "Advanced Methods for I/Q Imbalance Compensation in Communication Receivers,"*IEEE Trans. Signal Process*, vol. 49, no. 10, pp. 2335-2344, Oct 2001.

[18] A. Tarighat and A. H. Sayed, "MIMO OFDM receivers for Systems with IQ imbalances," *IEEE Trans. Signal Process*, vol. 53, no. 9, pp. 3583-3596, Sept. 2005.

[19] A. Hakkarainen, J. Werner, K. R. Dandekar and M. Valkama, "Analysis and Augmented Spatial Processing for Uplink OFDMA MU-MIMO Receiver With Transceiver I/Q Imbalance and External Interference," *IEEE Trans. Wireless Commun.*, vol. 15, no. 5, pp. 3422-3439, May 2016.

[20] N. Kolomvakis, M. Coldrey, T. Eriksson and M. Viberg, "Massive MIMO Systems With IQ Imbalance: Channel Estimation and Sum Rate Limits," *IEEE Trans. Commun.*, vol. 65, no. 6, pp. 2382-2396, June 2017.

[21] S. Zarei, W. H. Gerstacker, J. Aulin and R. Schober, "I/Q Imbalance Aware Widely-Linear Receiver for Uplink Multi-Cell Massive MIMO Systems: Design and Sum Rate Analysis," *IEEE Trans. Wireless Commun.*, vol. 15, no. 5, pp. 3393-3408, May 2016.

[22] J.K. Tugnait, "Multisensor detection of improper signals in improper noise", in *Proc. 2017 IEEE International Conference on Acoustics, Speech and Signal Processing (ICASSP)*, pp.3939 - 3943, 2017.

[23] L. Anttila, M. Valkama, and M. Renfors, "Circularity-based I/Q imbalance compensation in wideband direct-conversion receivers", *IEEE Trans. Veh. Technol.*, vol. 57, no. 4,pp.2099-2113, 2008.

[24] T. Adali, P.J. Schreier and L.L. Scharf, "Complex-valued signal processing: The proper way to deal with impropriety", *IEEE Trans. Signal Process.*, vol. 59, no. 11, pp.5101-5125, 2011.

[25] A. ElSamadouny, A. Gomaa and N. Al-Dhahir, "A Blind Likelihood-Based Approach for OFDM Spectrum Sensing in the Presence of I/Q Imbalance," *IEEE Trans. Commun.*, vol. 62, no. 5, pp. 1418-1430, May 2014.

[26] A. Gokceoglu, S. Dikmese, M. Valkama and M. Renfors, "Energy Detection under IQ Imbalance with Single- and Multi-Channel Direct-Conversion Receiver: Analysis and Mitigation," *IEEE J. Sel. Areas Commun.*, vol. 32, no. 3, pp. 411-424, March 2014.

[27] O. Semiari, B. Maham and C. Yuen, "On the Effect of I/Q Imbalance on Energy Detection and a Novel Four-Level Hypothesis Spectrum Sensing," *IEEE Trans. Veh. Technol.*, vol. 63, no. 8, pp. 4136-4141, Oct. 2014.

[28] A. A. A. Boulogeorgos, N. D. Chatzidiamantis and G. K. Karagiannidis, "Energy Detection Spectrum Sensing Under RF Imperfections," *IEEE Trans. Commun.*, vol. 64, no. 7, pp. 2754-2766, July 2016.

[29] A. Mehrabian and A. Zaimbashi, "Spectrum Sensing in SIMO Cognitive Radios Under Primary User Transmitter IQ Imbalance", *IEEE Systems Journal* vol. 13, no. 2, pp. 1210-1218, June 2019.

[30] A. Mehrabian and A. Zaimbashi, "GLRT-Based Spectrum Sensing for SIMO Cognitive Radio with Transmitter IQI", in *Proc. 2018 Iranian Conference on Electrical Engineering (ICEE)*, Mashhad, Iran, May 2018.

[31] E. Y. Imana, T. Yang and J. H. Reed, "Suppressing the Effects of Aliasing and IQ Imbalance on Multiband Spectrum Sensing," *IEEE Trans. Veh. Technol.*, vol. 66, no. 2, pp. 1074-1086, Feb. 2017.

[32] A. Mehrabian, and A. Zaimbashi, "Robust and Blind Eigenvalue-Based Multiantenna Spectrum Sensing Under IQ Imbalance", *IEEE Trans. Wireless Commun.*, vol. 17, no. 8, pp. 5581 - 5591, June 2018.

[33] B. Narasimhan, D. Wang, S. Narayanan, H. Minn, and N. Al-Dhahir, "Digital compensation of frequency-dependent joint Tx/Rx I/Q imbalance in OFDM systems under high mobility," *IEEE J. Sel. Topics Signal Process.*, vol. 3, no. 3, pp. 405417, Jun. 2009.

[34] S. John, "Some optimal multivariate tests", Biometrika, vol. 58, no. 1, pp. 123-127, 1971.

[35] L. Huang, C. Qian, Y. Xiao and Q. T. Zhang, "Performance analysis of volume-based spectrum sensing for cognitive radio," *IEEE Trans. Wireless Commun.*, vol. 14, no. 1, pp. 317-330, Jan. 2015.

[36] P.J. Schreier and L.L. Scharf, *Statistical Signal Processing of Complex-Valued Data*, Cambridge, U.K.: Cambridge Univ. Press., 2010.

[37] P. J. Schreier, "Bounds on the degree of impropriety of complex random bectors", *IEEE Signal Processing Lett.*, vol. 15, 2008.

[38] A. Zaimbashi, "Forward M-Ary Hypothesis Testing Based Detection Approach for Passive Radar" *IEEE Trans. Signal Process.*, vol. 65, no. 10, pp. 2659-2671, Feb. 2017.

[39] A. Zaimbashi, "Target Detection in Analogue Terrestrial TV-based Passive Radar Sensor: Joint Delay-Doppler Estimation," *IEEE Sensors J.*, vol.1, no.99, pp.1-1, 2017.

[40] A. Zaimbashi, "Broadband Target Detection Algorithm in FM-Based Passive Bistatic Radar Systems," *IET Radar, Sonar and Navigation*, vol.10, no.8, 1485-1499, 2016.

[41] G. Casella, and R.L. Berger, *Statistical inference*, Vol. 2, Pacific Grove, CA: Duxbury., 2002.

[42] A. Zaimbashi, "Invariant subspace detector in distributed multiple-input multiple output radar: Geometry gain helps improving moving target detection," *IET Radar, Sonar and Navigation*, vol.10, no.5, 923-934, 2016.

[43] E. Conte, A. De Maio, and C. Galdi, "CFAR detection of multidimensional signals: An invariant approach," *IEEE Trans. Signal Process.*, vol.51, no.1, 142-151, 2003.

[44] A. Zaimbashi, “Multiband FM-based passive bistatic radar: target range resolution improvement,” *IET Radar, Sonar and Navigation*, vol.10, no.1, 174-185, 2016.

[45] A. Ghobadzadeh, S. Gazor, M. Naderpour, and A.A. Tadaion, “Asymptotically optimal CFAR detectors,” *IEEE Trans. Signal Process.*, vol.64, no.4, 897-909, 2016.

Amir Zaimbashi (S’09–M’13) was born in Kerman, Iran, on January 20, 1981. He received the B.Sc. degree in electronics from Shahid Bahonar University of Kerman (SBUoK), Kerman, Iran, in 2004, the M.Sc. degree in communication systems from Yazd University, Yazd, Iran, in 2005, and the Ph.D. degree in communication systems from Shiraz University, Shiraz, Iran, in 2013. From 2006 to 2008, he was a researcher in digital signal processing with the Electrical and Computer Engineering Research Center, Isfahan University of Technology, Isfahan, Iran, working on the design and development stages of several communication systems. Since 2013, he has been with the Department of Electrical Engineering, Shahid Bahonar University of Kerman, Kerman, Iran, where he is currently an Associate Professor. He is the head of Optical and RF Communication Systems (ORCS) laboratory in SBUoK. His current research interests include statistical signal processing, array signal processing and optimization theory, and their applications in radar and wireless communication systems.

Mikko Valkama (S’00–M’01–SM’15) was born in Pirkkala, Finland, on November 27, 1975. He received the M.Sc. and Ph.D. Degrees (both with honors) in electrical engineering (EE) from Tampere University of Technology (TUT), Finland, in 2000 and 2001, respectively. In 2002, he received the Best Ph.D. Thesis -award by the Finnish Academy of Science and Letters for his dissertation entitled ”Advanced I/Q signal processing for wideband receivers: Models and algorithms”. In 2003, he was working as a visiting post-doc research fellow with the Communications Systems and Signal Processing Institute at SDSU, San Diego, CA. Currently, he is a Full Professor and Laboratory Head at the Laboratory of Electronics and Communications Engineering at TUT, Finland. His general research interests include radio communications, communications signal processing, estimation and detection techniques, signal processing algorithms for flexible radios, cognitive radio, full-duplex radio, radio localization, radio-based sensing and 5G mobile radio networks.